

Conformal Isometry of Lie Group Representation in Recurrent Network of Grid Cells

Dehong Xu^{1*}

xudehong1996@ucla.edu

Ruiqi Gao^{2*}

ruiqig@google.com

Wen-Hao Zhang³

Wenhao.Zhang@UTSouthwestern.edu

Xue-Xin Wei⁴

weixx@utexas.edu

Ying Nian Wu¹

ywu@stat.ucla.edu

¹Department of Statistics, UCLA ²Google Research, Brain Team

³Lyda Hill Department of Bioinformatics and O'Donnell Brain Institute, UT Southwestern Medical Center

⁴Departments of Neuroscience and Psychology, UT Austin

Abstract

The activity of the grid cell population in the medial entorhinal cortex (MEC) of the brain forms a vector representation of the self-position of the animal. Recurrent neural networks have been developed to explain the properties of the grid cells by transforming the vector based on the input velocity, so that the grid cells can perform path integration. In this paper, we investigate the algebraic, geometric, and topological properties of grid cells using recurrent network models. Algebraically, we study the Lie group and Lie algebra of the recurrent transformation as a representation of self-motion. Geometrically, we study the conformal isometry of the Lie group representation of the recurrent network where the local displacement of the vector in the neural space is proportional to the local displacement of the agent in the 2D physical space. We then focus on a simple non-linear recurrent model that underlies the continuous attractor neural networks of grid cells. Our numerical experiments show that conformal isometry leads to hexagon periodic patterns of the response maps of grid cells and our model is capable of accurate path integration.

1 Introduction

Grid cells [21, 16, 34, 25, 24, 9] in the mammalian medial entorhinal cortex (MEC) exhibit striking hexagon grid patterns when the agent (e.g., a rodent) navigates in 2D open environments [17, 21, 14, 5, 32, 4, 6, 8, 29, 1]. It is hypothesized that grid cell system is performing path integration [7, 12, 21, 13, 27, 20, 30, 23]. That is, the grid cells integrate self-motions of the animal over time to keep track of the self-position. This can be realized by a recurrent neural network, which takes the velocity of the self-motion as input, and transforms the activities of the grid cells based on the input velocity.

Collectively, the activities of the grid cell population form a vector in the high-dimensional neural activity space. This provides a representation of the self-position of the agent in space. The recurrent network transforms the vector based on the movement velocity of the agent, so that the transformation is a representation of self-motion, when considered from the perspective of representational learning. The vector and the transformation together form a representation of the 2D Euclidean group, which is an abelian additive Lie group.

*Equal contributions.

In a recent paper, [18] studied an isotropic scaling or conformal isometry property, and in the context of linear transformation models, connected this property to the hexagon periodic patterns of the grid cell response maps. With the conformal isometry property of the transformation of the recurrent network, the change of the vector in the neural space is proportional to the input velocity of the self-motion in the 2D physical space. [18] justified this condition in terms of robustness to errors or noises in the neurons. They studied a prototype model of linear recurrent network, which has an explicit algebraic and geometric structure in the form of a matrix group of rotations.

In this paper, we study conformal isometry in the context of the non-linear recurrent model that underlies the hand-crafted continuous attractor neural network (CANN) [5, 6, 29, 1]. In particular, we shall focus on the vanilla version of the recurrent network that is linear in the vector representation of self-position and is additive in the input velocity, followed by an element-wise non-linear rectification such as ReLU. This model has the simplicity that it is additive in input velocity before rectification. We also explore more complex variants for non-linear recurrent network, such as long short term memory network (LSTM) [22].

Our numerical experiments show that our conformal isometry condition is able to learn highly structured multi-scale hexagon grid patterns, consistent with the properties of experimentally observed grid cells from rodents. In addition, our learned model is also capable of accurate long-distance path integration. Our results generalize the previous results of linear network models ([18]) to an important class of non-linear network models in theoretical neuroscience that are more physiologically realistic.

2 Lie group representation and conformal isometry

2.1 Representations of self-position and self-motion

We start by introducing the basic components of our model. Let $\mathbf{x} = (x_1, x_2) \in \mathbb{R}^2$ be the self-position of the agent. Let $\Delta\mathbf{x} = (\Delta x_1, \Delta x_2)$ be the input velocity of the self-motion, i.e., displacement of the agent within unit time, so that the agent moves from \mathbf{x} to $\mathbf{x} + \Delta\mathbf{x}$ after unit time.

We assume $\mathbf{v}(\mathbf{x}) = (v_i(\mathbf{x}), i = 1, \dots, D)$ to be the vector representation of self-position \mathbf{x} , where each element $v_i(\mathbf{x})$ can be interpreted as the activity of a grid cell when the agent is at self-position \mathbf{x} . $(v_i(\mathbf{x}), \forall \mathbf{x})$ corresponds to the response map of grid cell i . D is the dimensionality of \mathbf{v} , i.e., the number of grid cells. We call the space of \mathbf{v} the “neural space”. The set $(\mathbf{v}(\mathbf{x}), \mathbf{x} \in \mathbb{R}^2)$ forms a 2D manifold, or an embedding of \mathbb{R}^2 , in the D -dimensional neural space. We call $(\mathbf{v}(\mathbf{x}), \mathbf{x} \in \mathbb{R}^2)$ the “coding manifold”.

With self-motion $\Delta\mathbf{x}$, the vector representation $\mathbf{v}(\mathbf{x})$ is transformed to $\mathbf{v}(\mathbf{x} + \Delta\mathbf{x})$ by a general transformation model:

$$\mathbf{v}(\mathbf{x} + \Delta\mathbf{x}) = F(\mathbf{v}(\mathbf{x}), \Delta\mathbf{x}) = F_{\Delta\mathbf{x}}(\mathbf{v}(\mathbf{x})), \quad (1)$$

where by simplifying $F(\cdot, \Delta\mathbf{x})$ as $F_{\Delta\mathbf{x}}(\cdot)$, we emphasize that the transformation F is dependent on $\Delta\mathbf{x}$. While $\mathbf{v}(\mathbf{x})$ is a representation of \mathbf{x} , $F_{\Delta\mathbf{x}}$ is a representation of $\Delta\mathbf{x}$. $(\mathbf{v}(\mathbf{x}), \forall \mathbf{x})$ and $(F_{\Delta\mathbf{x}}(\cdot), \forall \Delta\mathbf{x})$ together form a representation of the 2D additive Euclidean group \mathbb{R}^2 , which is an abelian Lie group. Specifically, we have the following group representation condition for the transformation model:

Condition 1. (*Algebraic condition on Lie group representation*). For any \mathbf{x} , we have (1) $F_0(\mathbf{v}(\mathbf{x})) = \mathbf{v}(\mathbf{x})$, and (2) $F_{\Delta\mathbf{x}_1 + \Delta\mathbf{x}_2}(\mathbf{v}(\mathbf{x})) = F_{\Delta\mathbf{x}_2}(F_{\Delta\mathbf{x}_1}(\mathbf{v}(\mathbf{x}))) = F_{\Delta\mathbf{x}_1}(F_{\Delta\mathbf{x}_2}(\mathbf{v}(\mathbf{x})))$ for any \mathbf{x} , $\Delta\mathbf{x}_1$ and $\Delta\mathbf{x}_2$.

Condition 1(1) requires that the coding manifold $(\mathbf{v}(\mathbf{x}), \forall \mathbf{x})$ are fixed points of F_0 with $\Delta\mathbf{x} = 0$. If F_0 is further an contraction off the coding manifold, then $(\mathbf{v}(\mathbf{x}), \forall \mathbf{x})$ are the attractor points of F_0 . Condition 1(2) requires that moving in one step with displacement $\Delta\mathbf{x}_1 + \Delta\mathbf{x}_2$ should be the same as moving in two steps with displacements $\Delta\mathbf{x}_1$ and $\Delta\mathbf{x}_2$ respectively. The group representation condition is the necessary condition for any valid transformation model (Equation (1)) of grid cells.

Group representation is a central theme in modern mathematics and physics [35]. However, most of the transformations studied in mathematics and physics are linear transformations that form matrix groups. [19] and [18] also focused on matrix groups, with $F_{\Delta\mathbf{x}}(\mathbf{v}(\mathbf{x})) = \mathbf{M}(\Delta\mathbf{x})\mathbf{v}(\mathbf{x})$, so that $\mathbf{M}(\Delta\mathbf{x}_1 + \Delta\mathbf{x}_2) = \mathbf{M}(\Delta\mathbf{x}_1)\mathbf{M}(\Delta\mathbf{x}_2) = \mathbf{M}(\Delta\mathbf{x}_2)\mathbf{M}(\Delta\mathbf{x}_1)$. Since the transformations in the recurrent neural networks are usually non-linear, we shall focus on non-linear transformations in this paper.

2.2 Conformal isometry

For an infinitesimal self-motion $\delta \mathbf{x}$, we can derive a first-order Taylor expansion of the transformation model in 1 with respect to $\delta \mathbf{x}$

$$\begin{aligned} \mathbf{v}(\mathbf{x} + \delta \mathbf{x}) &= F_0(\mathbf{v}(\mathbf{x})) + F'_0(\mathbf{v}(\mathbf{x}))\delta \mathbf{x} + o(|\delta \mathbf{x}|) \\ &= \mathbf{v}(\mathbf{x}) + f(\mathbf{v}(\mathbf{x}))\delta \mathbf{x} + o(|\delta \mathbf{x}|), \end{aligned} \quad (2)$$

where $f(\mathbf{v}(\mathbf{x})) = \frac{\partial F_{\Delta \mathbf{x}}}{\partial \Delta \mathbf{x}}(\mathbf{v}(\mathbf{x}))|_{\Delta \mathbf{x}=0}$ is a $D \times 2$ matrix.

While $(F_{\Delta \mathbf{x}}, \forall \Delta \mathbf{x} \in \mathbb{R}^2)$ forms an abelian Lie group, its derivative of $\Delta \mathbf{x}$ at 0, i.e., f , spans its Lie algebra. Both $F_{\Delta \mathbf{x}}$ and f are transformations acting on the coding manifold $(\mathbf{v}(\mathbf{x}), \forall \mathbf{x})$.

We identify the conformal isometry condition of the Lie group representation as follows:

Condition 2. (*Geometric condition on conformal isometry*).

$$f(\mathbf{v}(\mathbf{x}))^\top f(\mathbf{v}(\mathbf{x})) = s^2 \mathbf{I}_2, \forall \mathbf{x}, \quad (3)$$

where \mathbf{I}_2 is the 2-dimensional identity matrix. That is, the two column vectors of $f(\mathbf{v}(\mathbf{x}))$ are of equal norm s , and are orthogonal to each other.

Under the conformal isometry condition, $\mathbf{v}(\mathbf{x} + \delta \mathbf{x}) - \mathbf{v}(\mathbf{x}) \approx f(\mathbf{v}(\mathbf{x}))\delta \mathbf{x}$ is conformal to $\delta \mathbf{x}$, i.e., the 2D local Euclidean space of $(\delta \mathbf{x})$ in the physical space is embedded conformally as another 2D local Euclidean space $f(\mathbf{v}(\mathbf{x}))\delta \mathbf{x}$ in the neural space, and we only need to replace the two orthogonal axes for $\delta \mathbf{x}$ in the 2D physical space by the two column vectors of $f(\mathbf{v}(\mathbf{x}))$ in the neural space.

An equivalent statement for the conformal isometry condition is

$$\|\mathbf{v}(\mathbf{x} + \delta \mathbf{x}) - \mathbf{v}(\mathbf{x})\| = s\|\delta \mathbf{x}\| + o(\|\delta \mathbf{x}\|), \forall \mathbf{x}, \delta \mathbf{x}. \quad (4)$$

That is, the displacement in the neural space is proportional to the displacement in the 2D physical space.

Note that since our analysis is local, s may depend on \mathbf{x} . If s is a global constant, then the coding manifold $(\mathbf{v}(\mathbf{x}), \forall \mathbf{x})$ has a flat intrinsic geometry (imagining folding a piece of paper without stretching it).

[18] studied the conformal isometry property in a local polar coordinate system. In our definition above, we use 2D cartesian coordinate system, which is more convenient for the non-linear recurrent model. In the context of linear recurrent network, [18] linked the conformal isometry to the hexagon grid patterns of grid cells.

2.3 2D torus, 2D periodicity, and hexagon grid patterns

The 2D torus topology is commonly assumed *a priori* in the continuous attractor neural networks (CANN) for grid cells [5, 6, 29, 1]. Within our framework, we find that such a topology is in fact a theoretical consequence of abelian Lie group or the group representation condition (Condition 1). Specifically, since the elements of $\mathbf{v}(\mathbf{x})$ represent neuron activities, which are bounded biologically, the coding manifold $(\mathbf{v}(\mathbf{x}), \forall \mathbf{x})$ is bounded and compact, and therefore the group of $(F_{\Delta \mathbf{x}}, \forall \Delta \mathbf{x})$ is also compact. According to Lie group theory [11], if the abelian Lie group $(F_{\Delta \mathbf{x}}, \forall \Delta \mathbf{x})$ is compact and connected, then it has a topology of 2D torus, i.e., it is isomorphic to $\mathbb{S}_1 \times \mathbb{S}_1$, where \mathbb{S}_1 is a circle. Thus $(\mathbf{v}(\mathbf{x}) = F_{\mathbf{x}}(\mathbf{v}(0)), \forall \mathbf{x} \in \mathbb{R}^2)$ also forms a 2D torus.

While the group representation condition only gives us an algebraic structure, the conformal isometry condition (Condition 2) further fixes the geometry. Under the conformal isometry condition, if we further assume that the scaling factor s is a constant globally for all \mathbf{x} , then the intrinsic geometry of the coding manifold $(\mathbf{v}(\mathbf{x}), \forall \mathbf{x})$ remains Euclidean, and the coding manifold is a flat torus. That is, the coding manifold is not only isomorphic to $\mathbb{S}_1 \times \mathbb{S}_1$, but is also conformally isometric to $\mathbb{S}_1 \times \mathbb{S}_1$. While isomorphism is about mapping, isometry is about metric.

According to the theory of 2D Bravais lattice [2], we can find two primitive vectors $\Delta \mathbf{x}_1$ and $\Delta \mathbf{x}_2$, with $\|\Delta \mathbf{x}_1\| = \|\Delta \mathbf{x}_2\|$, and $\mathbf{v}(\mathbf{x} + k_1 \Delta \mathbf{x}_1 + k_2 \Delta \mathbf{x}_2) = \mathbf{v}(\mathbf{x})$ for arbitrary integers k_1 and k_2 . Along each primitive vector, for each period, $(\mathbf{v}(\mathbf{x} + c \Delta \mathbf{x}_i), c \in [0, 1])$ traces out a circle in the neural space for $i = 1, 2$, causing the periodicity in $\mathbf{v}(\mathbf{x})$. According to the theory of 2D Bravais lattice, the angle

between Δx_1 and Δx_2 can either be $\pi/2$ for square lattice or $2\pi/3$ for hexagon lattice. It is likely that the hexagon periodicity provides a better fit to place cells, in that the hexagon lattice provides denser packing of discrete Fourier components. We shall study this problem more rigorously in future work. It seems that hexagonal periodicity emerges under the general conditions of group representation and conformal isometry, independent of a specific form of the transformation model, as we observe empirically in the experiments (Section 5).

3 Non-linear recurrent neural network

3.1 Model

In this paper, we mainly focus on studying transformations $F_{\Delta x}(\cdot)$ that are locally approximated by non-linear recurrent neural networks. We start from assuming the following vanilla version of non-linear recurrent network:

$$v(x + \Delta x) = \text{ReLU}(\mathbf{W}v(x) + \mathbf{U}\Delta x), \quad (5)$$

where $\text{ReLU}(a) = \max(0, a)$ is applied element-wise, \mathbf{W} is a $D \times D$ weight matrix of recurrent connections, \mathbf{U} is a $D \times 2$ matrix, and the self-motion $\Delta x = (\Delta x_1, \Delta x_2)^\top$ is treated as 2×1 vector. Note that the above model is an accurate approximation to $F_{\Delta x}(\cdot)$ only for small Δx , as it may not satisfy Condition 1 in general for large Δx . Following Condition 1(1), for $\Delta x = 0$ we have $v(x) = \text{ReLU}(\mathbf{W}v(x))$. That is, the coding manifold $(v(x), \forall x)$ consists of the fixed points of $F_0(\cdot)$.

Compared to the matrix group in [18] where $F_{\Delta x}(v(x)) = \mathbf{M}(\Delta x)v(x)$, and $\mathbf{M}(\Delta x)$ is further derived as an exponential map that is highly non-linear in Δx , the above model (5) is much simpler and more biologically plausible in that, before ReLU, we have a single recurrent weight matrix \mathbf{W} that is independent of Δx , and Δx enters the equation additively. The ReLU rectification plays a critical role for the overall non-linear effect of Δx .

For this model, we can derive $f(v(x))$ as

$$f(v(x)) = \mathbf{1}(\mathbf{W}v(x) > \mathbf{0}) \odot \mathbf{U}, \quad (6)$$

where $\mathbf{1}(\cdot)$ is a vector of binary indicators calculated element-wise, and \odot is row-wise product. The indicator vector $\mathbf{1}(\mathbf{W}v(x) > \mathbf{0})$ changes as x changes, and it controls the change of v in the neural space according to Δx .

Since $\mathbf{1}(\cdot)$ is not differentiable, we propose to define the loss function to enforce the conformal isometry condition based on the equivalent statement in 4, as discussed in Section 4.2. In A.3, we also discuss a possible mechanism where conform isometry can be automatically satisfied by design.

Modules. Since it is well-known that biological grid cells are organized in discrete modules with different scales of patterns, we assume that in our model, the vector representations $v(x)$ are divided into sub-vectors analogous to modules, and accordingly the transformation is also module-wise by assuming \mathbf{W} is block-diagonal and \mathbf{U} is divided into sub-blocks by row.

More complex transformations. We also explore the Long Short-Term Memory network (LSTM) [22], a more complex variant of recurrent network, as the local transformation model. In the experiments, we observed learned hexagon grid patterns with the two types of transformation models, implying that the emergence of hexagonal periodicity under the conformal isometry condition can be agnostic to the specific form of the transformation model, at least empirically.

3.2 Eigen analysis

Next, we will deepen our theoretical understanding of the model (5) by conducting eigen analysis under the conformal isometry condition.

Theorem 1. *Under conformal isometry condition, for every x , the two columns of $\mathbf{1}(\mathbf{W}v(x) > \mathbf{0}) \odot \mathbf{U}$ are orthogonal, and they are eigenvectors of $\mathbf{1}(\mathbf{W}v(x) > \mathbf{0}) \odot \mathbf{W}$ with eigenvalue 1.*

See Appendix for a proof. If the magnitudes of all the other eigenvalues of $\mathbf{1}(\mathbf{W}v(x) > \mathbf{0}) \odot \mathbf{W}$ are less than 1, the recurrent network is a contraction off the coding manifold, which is similar to the eigen structures of general continuous attractor neural networks as shown in [15].

4 Reconstructing place cells and learning by numerical optimization

4.1 Place cells and decoding

Given the activities of grid cells \mathbf{v} , the agent needs to decode its current self-position, which is achieved by the interaction between grid cells and place cells. For open fields, we can model place cells [28] by Gaussian kernels and connect them to grid cells by the following model [10, 31]:

$$A(\mathbf{x}, \mathbf{p}) = \exp(-\|\mathbf{x} - \mathbf{p}\|^2 / 2\sigma^2) = \langle \mathbf{v}(\mathbf{x}), \mathbf{q}(\mathbf{p}) \rangle, \quad (7)$$

where $A(\mathbf{x}, \mathbf{p})$ is the response map (as a function of \mathbf{x}) of the place cell associated with the position \mathbf{p} . $A(\mathbf{x}, \mathbf{p})$ measures the adjacency of \mathbf{x} to \mathbf{p} . $\mathbf{q}(\mathbf{p})$ is the query vector of the place cell \mathbf{p} , which can be interpreted as connection weights between the grid cells and the place cell \mathbf{p} . For a vector \mathbf{v} , we can decode its position $\hat{\mathbf{x}}$ by

$$\hat{\mathbf{x}} = \arg \max_{\mathbf{p}} \langle \mathbf{v}, \mathbf{q}(\mathbf{p}) \rangle, \quad (8)$$

i.e., we choose the position \mathbf{p} that is closest to the position encoded by \mathbf{v} .

In model (7), $\mathbf{v}(\mathbf{x})$ generated by the transformation model serves as a set of basis functions to reconstruct the set of functions $A(\mathbf{x}, \mathbf{p}), \forall \mathbf{p}$. This is related to the Peter-Weyl theory [33], which generalizes the Fourier analysis to Lie group and shows that the basis functions arise from Lie group representation. $\mathbf{v}(\mathbf{x})$ can be used to reconstruct and interpolate value functions of \mathbf{x} in general. Peter-Weyl theory is about matrix Lie groups. In our work, we focus on non-linear transformation groups which can still generate basis functions.

4.2 Loss function

Assuming the kernel $A(\mathbf{x}, \mathbf{p})$ is given as in 7, we can learn the model by minimizing the following loss term:

$$L_1 = \sum_{t=1}^T \sum_{\mathbf{p}} \mathbb{E}_{\mathbf{x}, \Delta \mathbf{x}} [A(\mathbf{x} + \Delta \mathbf{x}_1 + \dots + \Delta \mathbf{x}_t, \mathbf{p}) - \langle F_{\Delta \mathbf{x}_t} \dots F_{\Delta \mathbf{x}_1}(\mathbf{v}(\mathbf{x})), \mathbf{q}(\mathbf{p}) \rangle]^2, \quad (9)$$

The learnable parameters includes $(\mathbf{v}(\mathbf{x}), \forall \mathbf{x})$, $(\mathbf{q}(\mathbf{p}), \forall \mathbf{p})$, and parameters in $F_{\Delta \mathbf{x}}$. The expectations are estimated by Monte Carlo samples from simulated trajectories. $A(\mathbf{x}, \mathbf{p})$ are Gaussian kernels with predefined σ . In practice, we add an additional zero-step version of L_1 , i.e. the expectation term changes to $[A(\mathbf{x}, \mathbf{p}) - \langle \mathbf{v}(\mathbf{x}), \mathbf{q}(\mathbf{p}) \rangle]^2$.

To ensure that the conformal isometry condition is satisfied, we add an extra loss term based on the equivalent statement of conformal isometry. Following 4, for simplicity, we first denote $s(\mathbf{x}, \Delta \mathbf{x}) = (\|\mathbf{v}(\mathbf{x}) - \mathbf{v}(\mathbf{x} + \Delta \mathbf{x})\| / \|\Delta \mathbf{x}\|)^2$. Then we propose a conformal isometry loss:

$$L_2 = \mathbb{E}_{\mathbf{x}, \Delta \mathbf{x}_1, \Delta \mathbf{x}_2} [s(\mathbf{x}, \Delta \mathbf{x}_1) - s(\mathbf{x}, \Delta \mathbf{x}_2)]^2, \quad (10)$$

where $\Delta \mathbf{x}_1$ and $\Delta \mathbf{x}_2$ are sampled such that they have the same length Δr but with different directions, i.e. $\Delta \mathbf{x}_1 = (\Delta r \cos \theta_1, \Delta r \sin \theta_1)$, $\Delta \mathbf{x}_2 = (\Delta r \cos \theta_2, \Delta r \sin \theta_2)$. Moreover, we add another regularization term to penalize $\|\mathbf{q}(\mathbf{p})\|^2$.

5 Experiments

We optimize the model with simulated trajectories as training data. The environment is assumed to be a $1\text{m} \times 1\text{m}$ squared open field, discretized to a 40×40 lattice. $\mathbf{v}(\mathbf{x})$ is of 1800 dimensions, which is partitioned into 150 modules with module size 12. For $A(\mathbf{x}, \mathbf{p})$, we use a Gaussian adjacency kernel with $\sigma = 0.07$. We train a 10-step recurrent network as the transformation model, i.e., $T = 10$ in the loss term L_1 .

For L_1 , the displacement of $\Delta \mathbf{x}_t$ is restricted to be smaller than 3 grids. For the range of Δr in L_2 , we hypothesize that it could be proportional to the scale of the module (i.e., s in 4), which is also reflected as the scale of the learned hexagon patterns. To this end, we adaptively adjust the upper bound of Δr for each module during training, based on the scale of the learned hexagon patterns at the current training stage. We average the scales of the learned patterns within each module to represent the scale of that module, and set the upper bound of Δr of the module with the largest average scale to 15 grids. The ranges of Δr for the remaining modules are adjusted accordingly based on their scales.

Table 1: Gridness scores and valid rates of grid cells of learned models.

| Model | Gridness score (\uparrow) | % of grid cells (\uparrow) |
|-------------|-------------------------------|--------------------------------|
| [3] (LSTM) | 0.18 | 25.20 |
| [31] (RNN) | 0.48 | 56.10 |
| Ours (RNN) | 0.77 | 72.5 |
| Ours (LSTM) | 0.73 | 68.8 |

5.1 Hexagon patterns

Figure 1 shows the learned firing patterns of $v(\mathbf{x}) = (v_i(\mathbf{x}), i = 1, \dots, d)$ over the 40×40 lattice of \mathbf{x} . We randomly select 16 modules out of 150 modules for visualization purposes. Each image corresponds to the response map of a grid cell. Every row shows the learned units belonging to the same module. Clear regular hexagon grid patterns emerge. The loss term for conformal isometry is critical. Without it, the learned response maps show stripe-like patterns. See Appendix for ablation results.

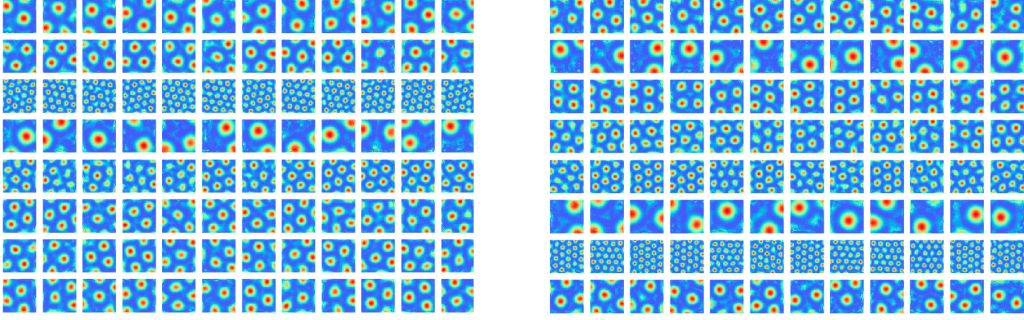


Figure 1: Hexagon grid firing patterns emerge in the learned $v(\mathbf{x})$. Each row represents the firing patterns of all the cells in the same module. Each unit shows the learned neuron activity over the whole 2D squared environment. The figure shows patterns from 16 randomly selected modules.

To quantitatively evaluate whether the learned patterns match regular hexagon grids, in Table 1, we report the gridness scores that are adopted from the literature of grid cells, as well as the valid percentage of grid cells with gridness score > 0.37 being the criteria. In Figure 2, we display the histogram of the spatial scales of the learned hexagon patterns. The multi-modal distribution is well fitted by a mixture of three Gaussians, which are centered at 0.41, 0.64 and 0.86 respectively. The ratios between adjacent centers are 1.55 and 1.35, which is consistent with the results from rodent grid cells.

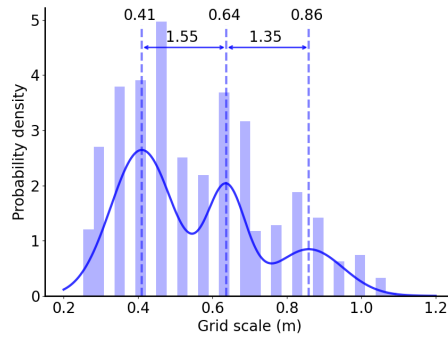


Figure 2: Histogram of grid scales of the learned model.

5.2 Path integration

We further test whether the learned model is capable of accurate path integration. We perform path integration in two scenarios. First, for path integration with re-encoding, we decode $v_t \rightarrow x_t$ to physical space and then apply encoder $v(x_t) \rightarrow v'_t$ back to neuron space every few steps. This re-encoding strategy helps correct the errors accumulated in the neural space along the transformation. In the without re-encoding case, we apply transformation purely using neuron vector v_t . As shown in the left subfigure of Figure 3, the model can perform near exact path integration for 30 steps (short distance) without re-encoding. For long-distance path integration, we train a 20-step recurrent network model, and evaluate the model for 500 steps over 1000 trajectories. As shown in the right subfigure of Figure 3, if we re-encode every 20 steps, the path integration error for the last step is 0.028, while the average error over the 500 steps trajectory is 0.017. Without re-encoding, the error is relatively larger, where the average error is around 0.03 along the whole trajectory, and 0.08 for the last step.

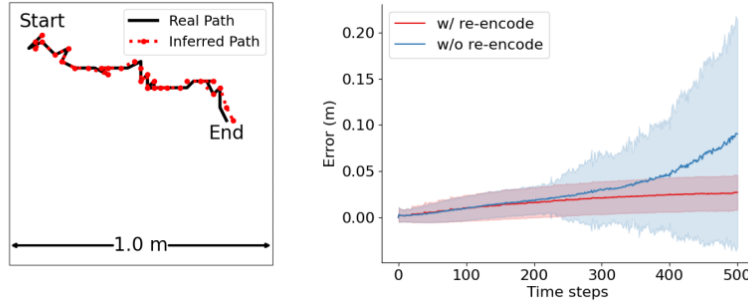


Figure 3: The learned model can perform accurate path integration. *Left*: path integration for 30 steps without re-encoding. The black trajectory is the ground truth and the red one is the inferred path by the learned model. *Right*: long distance (500-step) path integration error with (red) and without (blue) re-encoding by a learned 20-step RNN model over time steps. The average error and standard deviation are evaluated over 1000 trajectories.

To check if the model can apply precise encoding and decoding between physical space and neuron space, we also examine the fixed point condition by applying $v(x) \rightarrow v_t \rightarrow x'$. Ideally, the learned model can figure out the physical location x_t purely from v_t . The L_2 error between x and x' is nearly zero (< 0.005).

5.3 LSTM

In this section, we evaluate the LSTM transformation model. The model is still trained by the same loss functions as the vanilla RNN model. Meanwhile, we force $u > 0$ in training.

The learned patterns are partially visualized in Figure 4. Clear hexagon patterns also emerge. Different from the learned units from the vanilla recurrent network which are all non-negative, the learned $v(x)$ from the LSTM model can be either positive or negative, resulting in the color shift of the learned patterns. As shown in Table 1, the gridness score for LSTM model is 0.73 and there are 68.8% grid cells that are valid. We also evaluate the LSTM model on path integration still using 1000 trajectories. With re-encoding every 10 steps, the average error over the whole trajectory is 0.027, and the average error at 500 step still remains as low as 0.037.

6 Conclusion

This paper investigates the algebraic, geometric as well as topological properties of the transformation model of grid cells. We focus on non-linear recurrent neural networks under the conformal isometry condition. Our numerical experiments show that hexagon periodic patterns emerge in the response maps of grid cells under conformal isometry condition. Our experiments also show that the learned model is capable of accurate path integration.

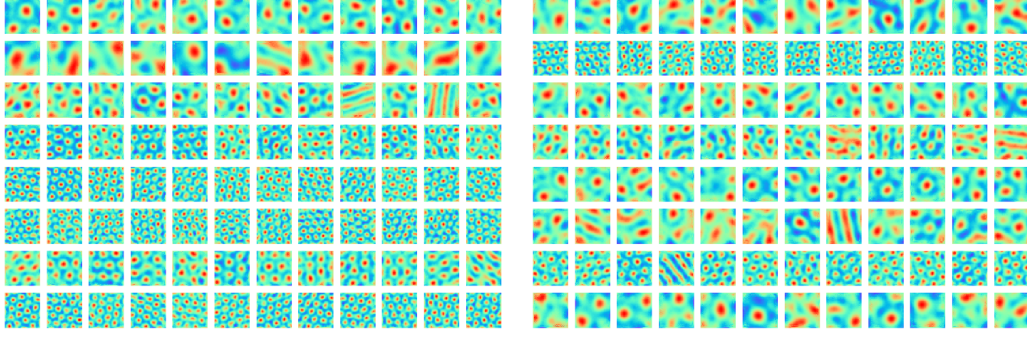


Figure 4: Learned hexagon grid patterns of $v(\mathbf{x})$ from the LSTM transformation model. For each row, it shows all the cells in the same module and 16 modules are randomly selected and visualized.

A limitation of our work is that we did not pursue specially designed recurrent neural networks where conformal isometry is automatically satisfied. We leave it to future investigation. In Appendix, we discuss a possible design inspired by the hand-crafted continuous attractor neural networks of grid cells where conformal isometry is satisfied.

References

- [1] Haggai Agmon and Yoram Burak. A theory of joint attractor dynamics in the hippocampus and the entorhinal cortex accounts for artificial remapping and grid cell field-to-field variability. *eLife*, 9:e56894, 2020.
- [2] Neil W Ashcroft, N David Mermin, et al. Solid state physics, 1976.
- [3] Andrea Banino, Caswell Barry, Benigno Uribe, Charles Blundell, Timothy Lillicrap, Piotr Mirowski, Alexander Pritzel, Martin J Chadwick, Thomas Degris, Joseph Modayil, et al. Vector-based navigation using grid-like representations in artificial agents. *Nature*, 557(7705):429, 2018.
- [4] Hugh T Blair, Adam C Welday, and Kechen Zhang. Scale-invariant memory representations emerge from moire interference between grid fields that produce theta oscillations: a computational model. *Journal of Neuroscience*, 27(12):3211–3229, 2007.
- [5] Yoram Burak and Ila R Fiete. Accurate path integration in continuous attractor network models of grid cells. *PLoS computational biology*, 5(2):e1000291, 2009.
- [6] Jonathan J Couey, Aree Witoelar, Sheng-Jia Zhang, Kang Zheng, Jing Ye, Benjamin Dunn, Rafal Czapkowski, May-Britt Moser, Edvard I Moser, Yasser Roudi, et al. Recurrent inhibitory circuitry as a mechanism for grid formation. *Nature neuroscience*, 16(3):318–324, 2013.
- [7] Charles Darwin. Origin of certain instincts, 1873.
- [8] Licurgo de Almeida, Marco Idiart, and John E Lisman. The input–output transformation of the hippocampal granule cells: from grid cells to place fields. *Journal of Neuroscience*, 29(23):7504–7512, 2009.
- [9] Christian F Doeller, Caswell Barry, and Neil Burgess. Evidence for grid cells in a human memory network. *Nature*, 463(7281):657, 2010.
- [10] Yedidyah Dordek, Daniel Soudry, Ron Meir, and Dori Derdikman. Extracting grid cell characteristics from place cell inputs using non-negative principal component analysis. *Elife*, 5:e10094, 2016.
- [11] William Gerard Dwyer and CW Wilkerson. The elementary geometric structure of compact lie groups. *Bulletin of the London Mathematical Society*, 30(4):337–364, 1998.
- [12] Ariane S Etienne and Kathryn J Jeffery. Path integration in mammals. *Hippocampus*, 14(2):180–192, 2004.
- [13] Ila R Fiete, Yoram Burak, and Ted Brookings. What grid cells convey about rat location. *Journal of Neuroscience*, 28(27):6858–6871, 2008.
- [14] Mark C Fuhs and David S Touretzky. A spin glass model of path integration in rat medial entorhinal cortex. *Journal of Neuroscience*, 26(16):4266–4276, 2006.
- [15] CC Alan Fung, KY Michael Wong, and Si Wu. A moving bump in a continuous manifold: a comprehensive study of the tracking dynamics of continuous attractor neural networks. *Neural Computation*, 22(3):752–792, 2010.

- [16] Marianne Fyhn, Torkel Hafting, Menno P Witter, Edvard I Moser, and May-Britt Moser. Grid cells in mice. *Hippocampus*, 18(12):1230–1238, 2008.
- [17] Marianne Fyhn, Sturla Molden, Menno P Witter, Edvard I Moser, and May-Britt Moser. Spatial representation in the entorhinal cortex. *Science*, 305(5688):1258–1264, 2004.
- [18] Ruiqi Gao, Jianwen Xie, Xue-Xin Wei, Song-Chun Zhu, and Ying Nian Wu. On path integration of grid cells: group representation and isotropic scaling. In *Neural Information Processing Systems*, 2021.
- [19] Ruiqi Gao, Jianwen Xie, Song-Chun Zhu, and Ying Nian Wu. Learning grid cells as vector representation of self-position coupled with matrix representation of self-motion. In *International Conference on Learning Representations*, 2019.
- [20] Mariana Gil, Mihai Ancau, Magdalene I Schlesiger, Angela Neitz, Kevin Allen, Rodrigo J De Marco, and Hannah Monyer. Impaired path integration in mice with disrupted grid cell firing. *Nature neuroscience*, 21(1):81–91, 2018.
- [21] Torkel Hafting, Marianne Fyhn, Sturla Molden, May-Britt Moser, and Edvard I Moser. Microstructure of a spatial map in the entorhinal cortex. *Nature*, 436(7052):801, 2005.
- [22] Sepp Hochreiter and Jürgen Schmidhuber. Long short-term memory. *Neural computation*, 9(8):1735–1780, 1997.
- [23] Aidan J Horner, James A Bisby, Ewa Zotow, Daniel Bush, and Neil Burgess. Grid-like processing of imagined navigation. *Current Biology*, 26(6):842–847, 2016.
- [24] Joshua Jacobs, Christoph T Weidemann, Jonathan F Miller, Alec Solway, John F Burke, Xue-Xin Wei, Nanthia Suthana, Michael R Sperling, Ashwini D Sharan, Itzhak Fried, et al. Direct recordings of grid-like neuronal activity in human spatial navigation. *Nature neuroscience*, 16(9):1188, 2013.
- [25] Nathaniel J Killian, Michael J Jutras, and Elizabeth A Buffalo. A map of visual space in the primate entorhinal cortex. *Nature*, 491(7426):761, 2012.
- [26] Diederik P Kingma and Jimmy Ba. Adam: A method for stochastic optimization. *arXiv preprint arXiv:1412.6980*, 2014.
- [27] Bruce L McNaughton, Francesco P Battaglia, Ole Jensen, Edvard I Moser, and May-Britt Moser. Path integration and the neural basis of the ‘cognitive map’. *Nature Reviews Neuroscience*, 7(8):663, 2006.
- [28] John O’Keefe. A review of the hippocampal place cells. *Progress in neurobiology*, 13(4):419–439, 1979.
- [29] Hugh Pastoll, Lukas Solanka, Mark CW van Rossum, and Matthew F Nolan. Feedback inhibition enables theta-nested gamma oscillations and grid firing fields. *Neuron*, 77(1):141–154, 2013.
- [30] Thomas Ridler, Jonathan Witton, Keith G Phillips, Andrew D Randall, and Jonathan T Brown. Impaired speed encoding is associated with reduced grid cell periodicity in a mouse model of tauopathy. *bioRxiv*, page 595652, 2019.
- [31] Ben Sorscher, Gabriel Mel, Surya Ganguli, and Samuel A Ocko. A unified theory for the origin of grid cells through the lens of pattern formation. 2019.
- [32] Sameet Sreenivasan and Ila Fiete. Grid cells generate an analog error-correcting code for singularly precise neural computation. *Nature neuroscience*, 14(10):1330, 2011.
- [33] Michael Taylor. Lectures on lie groups. *Lecture Notes*, available at <http://www.unc.edu/math/Faculty/met/lieg.html>, 2002.
- [34] Michael M Yartsev, Menno P Witter, and Nachum Ulanovsky. Grid cells without theta oscillations in the entorhinal cortex of bats. *Nature*, 479(7371):103, 2011.
- [35] Anthony Zee. *Group theory in a nutshell for physicists*. Princeton University Press, 2016.

A Appendix

A.1 More experimental details

A.1.1 Training details

We train the model for 200,000 iterations and learn the model by minimizing $L_1 + \lambda L_2$, where $\lambda = 0.05$. For the extra zero-step version of L_1 , the weight is set as 10. The regularization of $\|q(p)\|^2$ is added to the loss in the first 10,000 iterations, where we linearly decay the weight of the regularization from 0.1 to 0. For isometry loss (L_2), we fix the upper bounds of displacements as 15 grids for all modules for the first 10,000 iterations, and start to adaptively adjust the upper bounds afterwards every 2000 iterations. All the learned parameters are updated by Adam [26] optimizer. The learning rate is linearly decayed from 0.006 to 0.0003 for the first 10,000 iterations, fixed as 0.0003 until 120,000 iterations, and then linearly decayed to 0 afterwards. For batch sizes, we use 8000 for zero-step transformation loss and isometry loss (L_1), and 100 for multi-step transformation loss. We trained all the models on a single 2080 Ti GPU.

A.1.2 Learned patterns

In Figure 5, we show the autocorrelograms of the learned grid patterns from the vanilla recurrent network.

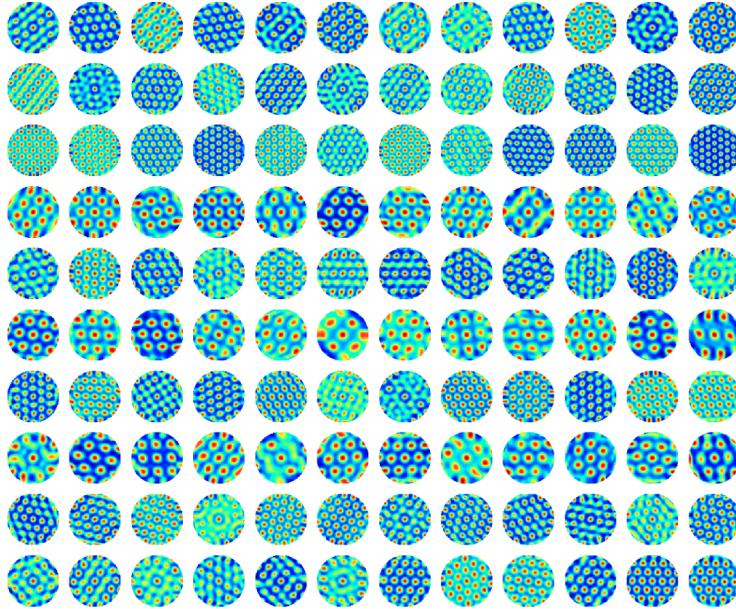


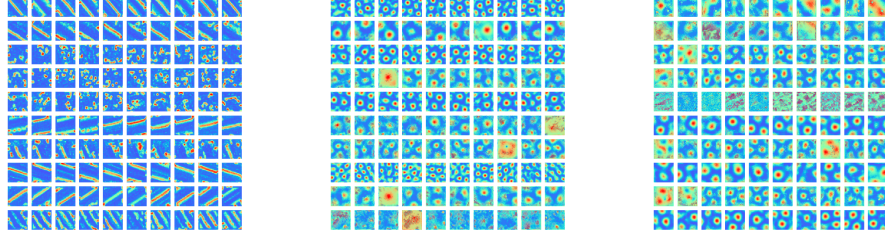
Figure 5: Autocorrelograms of the learned patterns.

A.1.3 Ablation studies

In this section, we present part of our ablation results to examine whether certain components of our model are empirically important for the emergence of hexagon grid patterns. Here are some key observations: (1) hexagon patterns don't emerge without conformal isometry loss. That is, the conformal isometry condition is crucial for the emergence of grid-like patterns. (2) Regularization of $\|q(p)\|^2$ is not necessary, but the patterns are less clear without it. (3) Without zero-step transformation loss, the learned model isn't able to path integrate accurately, although hexagon grid patterns still emerge.

We further try different module size. Figure 7 visualizes the learned patterns when we fix the total number of grid cells and change the module size to 24. It shows hexagonal grid firing patterns can emerge with larger module size. In Figure 8, we show the path integration error based on different

lengths (5-step, 10-step, 15-step and 30-step) of RNN models. Path integration for 30-step trajectories is performed to with and without re-encoding settings.



(a) Without isometry loss (b) Without regularization of \mathbf{u} (c) Without zero-step loss

Figure 6: Results of ablation on certain components of the training loss. (a) Learned patterns without conformal isometry loss. (b) Learned patterns without the regularization of $\|\mathbf{q}(\mathbf{p})\|^2$. (c) Learned patterns without zero-step transformation loss.

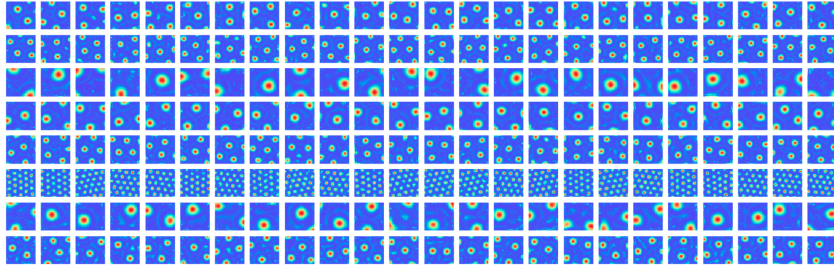


Figure 7: Learned patterns with module size 24.

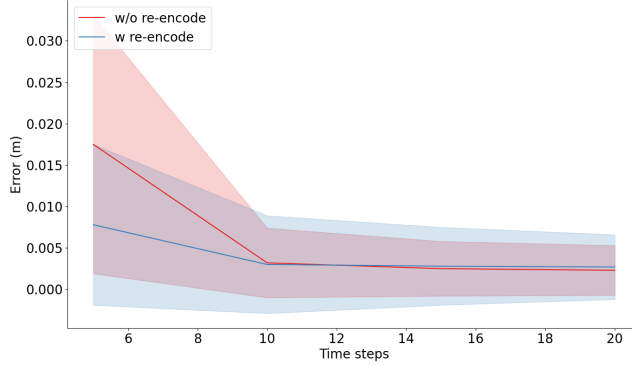


Figure 8: Path integration error over different lengths of RNN.

A.2 Eigen analysis

Proof. With $\Delta x = 0$, we have the following fixed point property:

$$\mathbf{v}(\mathbf{x}) = \text{ReLU}(\mathbf{W}\mathbf{v}(\mathbf{x})), \quad (11)$$

$$\mathbf{v}(\mathbf{x} + \delta\mathbf{x}) = \text{ReLU}(\mathbf{W}\mathbf{v}(\mathbf{x} + \delta\mathbf{x})). \quad (12)$$

Thus

$$\mathbf{v}(\mathbf{x} + \delta\mathbf{x}) - \mathbf{v}(\mathbf{x}) = \text{ReLU}(\mathbf{W}\mathbf{v}(\mathbf{x} + \delta\mathbf{x})) - \text{ReLU}(\mathbf{W}\mathbf{v}(\mathbf{x})) \quad (13)$$

$$= \mathbf{1}(\mathbf{W}\mathbf{v}(\mathbf{x}) > \mathbf{0}) \odot \mathbf{W}(\mathbf{v}(\mathbf{x} + \delta\mathbf{x}) - \mathbf{v}(\mathbf{x})) + o(|\delta\mathbf{x}|). \quad (14)$$

Thus for any \mathbf{x} , the matrix $\mathbf{1}(\mathbf{W}\mathbf{v}(\mathbf{x}) > \mathbf{0}) \odot \mathbf{W}$ has an eigenvalue 1 with geometric multiplicity 2. Meanwhile,

$$\mathbf{v}(\mathbf{x} + \delta\mathbf{x}) - \mathbf{v}(\mathbf{x}) = \text{ReLU}(\mathbf{W}\mathbf{v}(\mathbf{x}) + \mathbf{U}\delta\mathbf{x}) - \text{ReLU}(\mathbf{W}\mathbf{v}(\mathbf{x})) \quad (15)$$

$$= \mathbf{1}(\mathbf{W}\mathbf{v}(\mathbf{x}) > \mathbf{0}) \odot \mathbf{U}\delta\mathbf{x} + o(|\delta\mathbf{x}|). \quad (16)$$

Under conformal isometry, the two column vectors of $\mathbf{1}(\mathbf{W}\mathbf{v}(\mathbf{x}) > \mathbf{0}) \odot \mathbf{U}$ are orthogonal with equal norm, and they span the eigen-subspace of $\mathbf{1}(\mathbf{W}\mathbf{v}(\mathbf{x}) > \mathbf{0}) \odot \mathbf{W}$. \square

A.3 Discussion about conformal isometry

In our experiment, we impose conformal isometry with a loss term based on 4. In this section, we discuss a special case of the recurrent network that satisfies Condition 2 by design.

Specifically, we divide \mathbf{v} into low-dimensional sub-vectors, $\mathbf{v} = (\mathbf{v}_k, k = 1, \dots, K)$, where each \mathbf{v}_k is a sub-vector of dimension d , e.g., $d = 4$ so that each sub-vector consists of 4 neurons. We call each sub-vector a mini-block. Then the total dimension $D = Kd$. Such mini-blocks are commonly assumed in handcrafted continuous attractor neural networks [5, 6, 29, 1]. Correspondingly, we divide the $D \times 2$ matrix \mathbf{U} into K mini-blocks, with each being $d \times 2$, so that $\mathbf{U} = (\mathbf{U}_k, k = 1, \dots, K)$. The indicator vector $\mathbf{1}(\mathbf{W}\mathbf{v}(\mathbf{x}) > \mathbf{0})$ is also divided into K mini-blocks, each of dimension d .

We assume the following two conditions for the mini-blocks:

Condition 3. (*Orthogonality condition*). Each \mathbf{U}_k has two column vectors that are of equal norm s_k and are orthogonal to each other, i.e., $\mathbf{U}_k^\top \mathbf{U}_k = s_k^2 \mathbf{I}_2$.

The above condition can be easily satisfied, e.g., for $d = 4$, we let the first column of \mathbf{U}_k be $[1, 0, -1, 0]^\top$ and the second column be $[0, 1, 0, -1]^\top$. The idea is that within each mini-block, the cells are sensitive to different directions of self-motion.

Condition 4. (*Synchronicity condition*). Each mini-block of $\mathbf{1}(\mathbf{W}\mathbf{v}(\mathbf{x}) > \mathbf{0})$ is synchronized, i.e., all its elements are either all 0 or all 1. For mini-block k , define $a_k = 1$ if all the elements of $\mathbf{1}(\mathbf{W}\mathbf{v}(\mathbf{x}) > \mathbf{0})$ are 1, and $a_k = 0$ if all the elements of $\mathbf{1}(\mathbf{W}\mathbf{v}(\mathbf{x}) > \mathbf{0})$ are 0.

We call the mini-blocks that satisfy the above two conditions the conformal mini-blocks. Given those two conditions, we have the following result.

Theorem 2. *Under the orthogonality condition and the synchronicity condition, the mini-block-wise recurrent network satisfies the conformal isometry condition (Condition 2).*

Proof. The change of the vector

$$\mathbf{v}(\mathbf{x} + \delta\mathbf{x}) - \mathbf{v}(\mathbf{x}) = \mathbf{1}(\mathbf{W}\mathbf{v}(\mathbf{x}) > \mathbf{0}) \odot \mathbf{U}\delta\mathbf{x} + o(|\delta\mathbf{x}|). \quad (17)$$

Thus

$$\|\mathbf{v}(\mathbf{x} + \delta\mathbf{x}) - \mathbf{v}(\mathbf{x})\|^2 = \sum_k a_k s_k^2 \|\delta\mathbf{x}\|^2 + o(\|\delta\mathbf{x}\|^2) = s^2 \|\delta\mathbf{x}\|^2 + o(\|\delta\mathbf{x}\|^2), \quad (18)$$

where $s^2 = \sum_k a_k s_k^2$. \square

Define the activation pattern of $\mathbf{1}(\mathbf{W}\mathbf{v}(\mathbf{x}) > \mathbf{0})$ be $\mathbf{a}(\mathbf{x}) = (a_k, k = 1, \dots, K)$. $\mathbf{a}(\mathbf{x})$ controls the change of the vector $\mathbf{v}(\mathbf{x} + \delta\mathbf{x}) - \mathbf{v}(\mathbf{x})$. At different \mathbf{x} , $\mathbf{a}(\mathbf{x})$ are different. Thus the direction of the change $\mathbf{v}(\mathbf{x} + \delta\mathbf{x}) - \mathbf{v}(\mathbf{x})$ depends on \mathbf{x} , and it is possible for the model to create rotation of the vector $\mathbf{v}(\mathbf{x})$.